Physicochemical, structural and biological characterisation of poly(3-hydroxyoctanoate) supplemented with diclofenac acid conjugates - Harnessing the potential in the construction...

Article *in* International Journal of Biological Macromolecules · April 2024

DOI: 10.1016/j.ijbiomac.2024.131476

10 authors, including:

Katarzyna Haraźna
Cracow University of Technology
18 PUBLICATIONS **167** CITATIONS
SEE PROFILE

Rafał Konefał
The Czech Academy of Sciences
105 PUBLICATIONS **1,673** CITATIONS
SEE PROFILE

Bartosz Leszczynski
Jagiellonian University
46 PUBLICATIONS **384** CITATIONS
SEE PROFILE

Andrzej Wrobel
Jagiellonian University
77 PUBLICATIONS **614** CITATIONS
SEE PROFILE

International Journal of Biological Macromolecules 268 (2024) 131476

Contents lists available at ScienceDirect

International Journal of Biological Macromolecules

journal homepage: www.elsevier.com/locate/ijbiomac

Physicochemical, structural and biological characterisation of poly (3-hydroxyoctanoate) supplemented with diclofenac acid conjugates — Harnessing the potential in the construction of materials for skin regeneration processes

Katarzyna Haraźna [a,b,c,*,**,***], Annabelle T. Fricker [d], Rafał Konefał [e], Aneta Medaj [f,g], Małgorzata Zimowska [a], Bartosz Leszczyński [h], Andrzej Wróbel [h], Andrzej J. Bojarski [i], Ipsita Roy [d], Maciej Guzik [a,****]

[a] Jerzy Haber Institute of Catalysis and Surface Chemistry, Polish Academy of Sciences, Niezapominajek 8, 30-239 Kraków, Poland
[b] Łukasiewicz Research Network – Kraków Institute of Technology, Zakopiańska 73, 30-418 Kraków, Poland
[c] Department of Materials Engineering, Cracow University of Technology, 37 Jana Pawła II Av., 31-864 Kraków, Poland
[d] Department of Materials Science and Engineering, The University of Sheffield, Sheffield S3 7HQ, United Kingdom
[e] Institute of Macromolecular Chemistry, Czech Academy of Sciences, Heyrovského nám. 2, 162 06 Prague 6-Brevnov, Czech Republic
[f] Faculty of Chemistry, Jagiellonian University, Gronostajowa 2, 30-387 Kraków, Poland
[g] Doctoral School of Exact and Natural Sciences, Jagiellonian University, Łojasiewicza 11, 30-348 Kraków, Poland
[h] Faculty of Physics, Astronomy and Applied Computer Science, Jagiellonian University, Łojasiewicza 11, 30-348 Kraków, Poland
[i] Maj Institute of Pharmacology, Polish Academy of Sciences, Smętna 12, 31-343 Kraków, Poland

ARTICLE INFO

Keywords:
Polyhydroxyalkanoates
Poly(3-hydroxyoctanoate)
Artificial skin substitute, bioresorbable, porous layer of dressing material
Targeted delivery of diclofenac

ABSTRACT

This study involved creating oligomeric conjugates of 3-hydroxy fatty acids and diclofenac, named Dic-oligo (3HAs). Advanced NMR techniques confirmed no free diclofenac in the mix. We tested diclofenac release under conditions resembling healthy and chronic wound skin. These oligomers were used to make P(3HO) blends, forming patches for drug delivery. Their preparation used the solvent casting/porogen leaching (SCPL) method. The patches' properties like porosity, roughness, and wettability were thoroughly analysed. Antimicrobial assays showed that Dic-oligo(3HAs) exhibited antimicrobial activity against reference (*S. aureus, S. epidermis, S. faecalis*) and clinical (*Staphylococcus* spp.) strains. Human keratinocytes (HaCaT) cell line tests, as per ISO 10993-5, showed no toxicity. A clear link between material roughness and HaCaT cell adhesion was found. Deep cell infiltration was verified using DAPI and phalloidin staining, observed under confocal microscopy. SEM also confirmed HaCaT cell growth on these scaffolds. The strong adhesion and proliferation of HaCaT cells on these materials indicate their potential as wound dressing layers. Additionally, the successful diclofenac release tests point to their applicability in treating both normal and chronic wounds.

1. Introduction

The skin – the main barrier of the human body – is the tissue that covers the largest surface area of the body. Tissue damage and skin injuries happen to people of all ages [1]. Wound healing is a multilevel biochemical process occurring in response to physical tissue damage, with the following phases overlapping: haemostasis, inflammation, proliferation and reconstruction (scar formation) [2]. Inflammation usually results in the body's response to the presence of pathogens, including bacteria, viruses, and fungi. Interactions between antigens and

* Correspondence to: K. Haraźna, Department of Materials Engineering, Cracow University of Technology, 37 Jana Pawła II Av., 31-864 Kraków, Poland
** Correspondence to: K. Haraźna, Lukasiewicz Research Network – Krakow Institute of Technology, Zakopiańska 73, 30-418 Kraków, Poland
*** Correspondence to: K. Haraźna, Jerzy Haber Institute of Catalysis and Surface Chemistry, Polish Academy of Sciences, Niezapominajek 8, 30-239 Kraków, Poland.
**** Corresponding author.
E-mail addresses: katarzyna.harazna@pk.edu.pl (K. Haraźna), maciej.guzik@ikifp.edu.pl (M. Guzik).

https://doi.org/10.1016/j.ijbiomac.2024.131476
Received 5 January 2024; Received in revised form 27 March 2024; Accepted 6 April 2024
Available online 16 April 2024

antibodies, as well as oxidative stress, can also be factors that induce the inflammatory process. During this process, the enzyme phospholipase A2, present in leukocytes and platelets, is activated by pro-inflammatory cytokines. This is followed by hydrolysis of phospholipids from the damaged cell membrane, resulting in the synthesis of arachidonic acid. This product is a substrate for cyclooxygenases (COX) and lipoxygenases (LOX), which produce inflammatory metabolites: leukotrienes, prostaglandins and thromboxanes [3,4].

Traditional anti-inflammatory therapies are associated with the neutralisation or reduction of pro-inflammatory mediators and the inhibition of the involvement of leukocytes. To achieve this, compounds with anti-inflammatory properties, glucocorticoid receptor antagonists, antibodies, or inhibitors that inhibit pro-inflammatory cytokines are used, that is, TNF-α and various interleukins (ILs) [5]. Non-steroidal anti-inflammatory drugs (NSAIDs) are compounds taken to reduce pain, inflammation, or lower fever. NSAIDs inhibit the COX enzyme, which converts arachidonic acid into prostanoids, i.e. prostaglandins. Traditional non-selective COX inhibitors include aspirin, diclofenac (DIC), ibuprofen, and piroxicam [5]. Through inhibition of COX, DIC leads to a reduction in the prostaglandins responsible for inflammation and pain. It is commonly used systemically to treat postoperative pain [6]. Furthermore, literature reports indicate an antimicrobial effect of DIC. It is increasingly used in formulations to improve its bioavailability, allowing it to act through the skin coatings [7].

Modern skin substitutes should contribute to faster wound closure, restoring the barrier function of the wound while preventing the spread of inflammation and bacterial infection [8]. The interdisciplinary field known as tissue engineering can offer materials with the appropriate properties for regenerating skin e.g., dressings characterised by high porosity, which enables cell adhesion and proliferation, and also allows the transport of nutrients during tissue regeneration processes. The selection of an appropriate methodology and proper skin composition regeneration materials makes it possible to obtain the most optimal biochemical and mechanical properties, leading to increased adhesion, differentiation and proliferation of skin-building cells (e.g., keratinocytes or fibroblasts) [9,10]. A particularly interesting polymer derived through biotechnological processes, which the FDA has approved as a material for the construction of components for medical applications, is poly(4-hydroxybutyrate) [P(4HB)] [11]. This is related to the hydrolytic degradation of this polymer, occurring inside the human body, leading to the release of 4-hydroxycarboxylic acid molecules, which are characterised by moderate acidity (pKa = 4.84) [12]. P(4HB) represents a group of polyesters synthesised by bacterial fermentations – the polyhydroxyalkanoates (PHAs). In vivo studies of PHAs have shown that these polymers are slowly degraded, and their decomposition products are well metabolised by cells [11]. Considering the above, many research groups are investigating using polymers from the PHAs family, other than P(4HB), for constructing materials for medical applications. Due to the abovementioned characteristics, these polymers can be used to build drug carriers, materials for implant applications (i.e., stents, bone and nerve tissue regeneration materials), or dressing materials [12–27]. In the literature, there are several papers describing the possibility of using polymers of the PHA family and copolymers [e.g., P(4HB) or P(3HB-*co*-3HHx)] in the construction of dressing materials. Native unmodified porous structures made from P(3HB)/P(3HB-*co*-3HHx) blends by induced thermal phase separation were tested for use in skin regeneration. The study was conducted in an in vitro model using human keratinocyte (HaCaT) cells. The results showed that HaCaT can adhere and proliferate on the surface of the prepared scaffolds. Moreover, the porous structure of the materials promoted the production of collagen, which is one of the components of the extracellular matrix (ECM) [23]. Additionally, dressing materials prepared with PHA can also be trifunctional. This means that they can act: (1) as a barrier to protect the wound: (2) to stimulate regeneration of the wound site; and (3) as biosensors to detect bacterial infections. Such functional materials were made by Ward et al. using mcl-PHA and graphene. The dressing allowed the detection of pyocyanin, which is a secondary metabolite produced by *P. aeruginosa* [22].

Herein we show the possibility of using poly(3-hydroxyoctanoate) [P(3HO)] in the construction of a component of dressing materials, and P(3HO) supplemented with diclofenac-modified oligomers [Dic-oligo(3HAs)] in the preparation of analogous materials for the local delivery of active substances. The release profiles of DIC from the prepared carriers and kinetic models describing how it is delivered to the wound site are presented. The prepared biomaterials were characterised by a porous structure generated by the solvent casting/particulate leaching (SCPL) technique. In the presented work, the surface and mechanical properties of the prepared porous patches were evaluated. The results were correlated with information from in vitro bioassays for the HaCaT cell line and the findings from antimicrobial tests performed for reference and clinical strains. The thorough characterisation of the prepared biomaterials made it possible to assess their potential for biomedical applications.

2. Materials and methods

2.1. Materials

Materials are shown in the *Supporting Information* (paragraph S1.1).

2.2. Synthesis of Dic-oligo(3HAs)

The selection of the most favourable reaction parameters for the preparation of Dic-oligo(3HAs) is described in the *Supporting Information* (paragraph S1.2). *Procedure for preparing the final mixture containing Dic-oligo(3HAs)*: For synthesis the final mixture [Dic-oligo(3HAs)], the following reagents were used: P(3HO), 15 % of p-TSA and 40 % of DIC. The synthesis were carried out at 125 °C for 2 min once the melting of the reagents was observed. To obtain a reaction product that did not contain the free unreacted DIC, after washing the reaction mixture (dissolved in chloroform) with 1 M NaCl (x 4) and H_2O (x 2), as well as evaporating the chloroform (700 mbar, 25 °C), the reaction mixture was again dissolved in hexane. The solution was then alkalised by adding an aqueous NaOH solution. Then, the mixture was washed several times with 1 M NaCl and distilled water until a neutral pH was obtained (the pH value was measured with a universal indicator paper). The hexane was then evaporated from the reaction mixture under reduced pressure (350 mbar, 45 °C). The final reaction mixture was placed in a vacuum dryer for three days at 45 °C (Binder, Tuttlingen, Germany). The reaction product was obtained in three replicates.

2.3. Preparation of analysed materials

Synthesis of blends containing Dic-oligo(3HAs): P(3HO)/Dic-oligo(3HAs) are shown in the Supporting Information (paragraph S1.3). *Preparation of the porous patches*: The SCPL technique was used to obtain porous materials. For this purpose, sodium chloride with 100–300 μm grains was used. To obtain porous patches, 5 % (*w/v*) solutions of P(3HO) or P(3HO)/Dic-oligo(3HAs) were used, which were prepared by dissolving them in ethyl acetate. The amounts of polymer and NaCl used to produce the suspensions are shown in Table 1. The obtained suspensions were stirred overnight at room temperature. The mixtures were poured into suitable vessels and left for 14 days to evaporate the solvent and crystallise the polymer/blend. Afterwards, the materials were washed with distilled water, which was replaced 1–2 times daily. This porogen leaching process was carried out for six days. The remaining water was removed from the material by freeze-drying (Labconco, MO, USA). The prepared patches were stored in leak-proof vessels at 4 °C. The patches were obtained in at least three replicates.

Table 1
The amounts of reagents used in preparing the porous patches and the terminology used.

	Amount of P(3HO) or P(3HO)/Dic-oligo (3HAs) blends (%)	Amount of NaCl (%)
5P(3HO)	5	95
5P(3HO)/Dic-oligo (3HAs)	5	95
15P(3HO)	15	85
15P(3HO)/Dic-oligo(3HAs)	15	85
25P(3HO)	25	75
25P(3HO)/Dic-oligo(3HAs)	25	75

2.4. Methods

Spectroscopic analysis: The characterisation details of the spectroscopic methods (^{13}C NMR, COSY, HMBC, HSQC, ESI-MS) of the final reaction mixture are described in the *Supporting Information* (paragraph S1.4.1). *Release of DIC and kinetics*: The measurements for determining the release profiles of DIC and/or its esters (DIC/3HAs) are shown in the *Supporting Information* (paragraph S1.4.2 and 1.4.3). *Surface properties of Dic-oligo(3HAs):* The precise methodology for determining the wetting angles and surface free energies of the materials are described in the *Supporting Information* (paragraph S1.4.4). *Structural analysis of the prepared patches*: For the exact information regarding the implementation of the analyses, that is, computed microtomography (μ-CT), atomic force microscopy (AFM) and mechanical testing, please see the *Supporting Information* (paragraph S1.4.5). Minimal inhibitory concentrations (MIC_{90}) of DIC and Dic-oligo(3HAs) were determined against bacterial strains based on CLSI recommendations, with some modifications using the standard microdilution method. The above-mentioned strain were Gram-negative bacteria: *Escherichia coli* (NCTC 10538), *Klebsiella pneumoniae* (ATCC 10031), *Pseudomonas aeruginosa* (ATCC 27853), and Gram-positive bacteria: *Staphylococcus aureus* (ATCC 6538P, ATCC 25923), *Staphylococcus epidermidis* (RP62A), *Enterococcus faecalis* (ATCC 29212). Test concentrations of the compounds were from 800.00 to 6.25 $\mu g \cdot mL^{-1}$ and from 10.00 to 0.04 $mg \cdot mL^{-1,}$ for DIC and Dic-oligo (3HAs), respectively. The antimicrobial activity assay was carried out on their methanolic solutions, which were then diluted in Mueller Hinton broth (final methanol concentration was 0.5 %). Unmodified oligomers were tested as a negative control. All tests were performed in triplicate. The analysis of the growth rate of clinical strains: Two clinical strains of *Staphylococcus* spp. such as *S. epidermidis* O–121 and O–202 were tested. Briefly, microplates were incubated with bacteria at a concentration of 5×10^5 $CFU \cdot mL^{-1}$. Then, an appropriate amount of Dic-oligo(3HAs) was added to the mixture. The plates were then incubated with shaking at 37 °C and 200 rpm for 20 h. During the experiment, optical density (OD) was measured automatically every 5 min. As a negative control, the MH broth with a final concentration of methanol 0.5 % as a oligomer solvent were used. Assays were repeated three times. *Biological tests* in vitro*:* The details of the in vitro cell culture conditions for HaCaT cells and the preparation of the materials for cell culture are described in the *Supporting Information* (paragraph S1.4.6.1). *Indirect cytotoxicity tests:* The experiments were carried out in accordance with ISO 10993–5:2009 using extracts obtained by incubating the prepared patches in Dulbecco's Modified Eagle's Medium (DMEM) for 24 h. The extracts were obtained according to ISO 10993–12, where 40 mg of the appropriate biomaterial was incubated in 1 mL of DMEM for 24 h, at 37 °C, in an atmosphere containing 5 % CO_2. At the same time, HaCaT were seeded into 96-well plates at a concentration of 2×10^4 cells per well, and then were incubated in a 200 μL medium. Afterwards, the prepared plates were placed in an incubator for 24 h, at 37 °C, in an atmosphere containing 5 % CO_2. After the time above, the DMEM was removed and replaced with the same volume of the obtained extracts (200 μL). The prepared plates were again placed in the incubator for 24 h, maintaining the same culture conditions. After the incubation period, a positive control was prepared. For this purpose, the medium in the dedicated wells was replaced with 0.1 % (*v*/v) triton X-100 for 15 min. After the mentioned time, the cells were washed with PBS solution. In the experiment, the wells in which the cells were in contact with DMEM only were used as a negative control. For the exact information regarding the *resazurin spectrophotometric assay* please see the *Supporting Information* (paragraph S1.4.6.2). *Live/Dead assay:* In these experiments, 15×10^4 cells/well were seeded in 6-well plates. The cells were incubated in 2 mL of DMEM for 24 h at 37 °C in an atmosphere containing 5 % CO_2. After 24 h, the DMEM was removed from the wells and replaced with an equal volume of the corresponding extracts (for the procedure for obtaining them: see above). The prepared plates were again placed in an incubator for 24 h (37 °C, 5 % CO_2). The positive and negative controls were prepared analogously to the abovementioned experiment. Solutions of calcein green AM (2 $\mu L \bullet mL^{-1}$ in DMSO) and ethidium bromide (0.1 $\mu L \bullet mL^{-1}$ in PBS) were prepared to start the double staining assay. The cells were incubated with the prepared solutions in the dark for 30 min, at 37 °C, in an atmosphere containing 5 % CO_2. Afterwards, the cells were observed using a fluorescence microscope (Olympus IX3, Tokyo, Japan). *Direct bioassays performed in contact with the surface of biomaterials:* The procedure for preparing patches for direct contact and proliferation testing is detailed in the *Supporting Information* (paragraph S1.4.6.3). *Direct cytotoxicity tests:* 10^5 cells were placed on the surface of each prepared material. Each well of the plates was supplemented with 4 mL of DMEM. Then, the prepared materials were incubated for two days at 37 °C in an atmosphere containing 5 % CO_2. After this time, the cells on the scaffolds were stained using the Live/Dead staining methodology. The scaffolds were washed several times with PBS and incubated with the prepared fluorescent dye solutions in the dark for 30 min, at 37 °C, in an atmosphere containing 5 % CO_2. The cells were then observed using a confocal scanning microscope (Zeiss LSM510-META, UK) with an argon-ion laser. Recording of the stained structures was made possible using the following parameters: excitation/emission at 494/517 nm: green fluorescence – living cells; excitation/emission at 517/617 nm: red fluorescence – dead cells. *Direct proliferation test (spectrophotometric resazurin test):* On the surface of the scaffolds, 10^4 of the HaCaT, resuspended in 30 μL of DMEM, were seeded. The plates prepared this way were placed for 30 min in a culture incubator at 37 °C in an atmosphere containing 5 % CO_2. After this, the volume of DMEM was completed to 1 mL per well. The blank solutions, native DMEM, were incubated in three wells. The culture plates were incubated for 14 days (37 °C, 5 % CO_2). The DMEM was removed from the culture plates every three days and replaced with fresh reagent. On the experiment's 1st, 3rd, 8th, 11th and 14th days, the number of cells on the scaffolds were determined using a spectrophotometric assay based on resazurin reduction (please see the *Supporting Information*: paragraph S1.4.6.2). *Direct proliferation tests (Live/Dead staining):* On the 14th day of the experiment described above, the scaffolds were transferred from 24-well to 6-well plates. The scaffolds were then washed with PBS and incubated with calcein green AM (2 $\mu L \bullet mL^{-1}$ in DMSO) and ethidium bromide (0.1 $\mu L \bullet mL^{-1}$ in PBS) staining solutions for 30 min (37 °C, 5 % CO_2). The procedure for materials preparation and analysis using the confocal microscope is described in the section: *Direct cytotoxicity tests*. *Staining of cytoskeleton elements of cells:* After the 14th day of direct proliferation assays, the cells on the scaffolds were dehydrated by incubation in 3.7 % formaldehyde. Afterwards, the cells were washed several times with PBS, followed by immersion in 0.1 % (*v*/v) Triton X-100 for 20 min. In the next step, the cells were again washed several times with PBS, after which they were incubated in a solution of tetramethylrhodamine (TRITC) labelled phalloidin (1/500, diluted in PBS) and 4′,6-diamidino-2-phenylindole: DAPI (1/1000, diluted in PBS) for 30 min, in the dark. After this, the materials were washed several times with PBS and then observed using a confocal scanning microscope (Zeiss LSM510-META, Zeiss, UK) equipped with an argon-ion laser and a two-photon Ti-

Sapphire. Recording of the stained structures was made possible using the following parameters: excitation/emission at 517/617 nm, red fluorescence – TRITC; excitation/emission at 800/470 nm, blue fluorescence – DAPI. *Observation of cell morphology on scaffolds:* After the direct proliferation assays on the 1st and 14th days, the cells were fixed by impregnating them twice in 4 % (*v*/v) formaldehyde. Then, the cells deposited on the surface of the materials were gradually dehydrated by immersing the scaffolds for 15 min in aqueous ethanol solutions at the following concentrations: 35 %, 50 %, 70 % and 90 %. The final step was to immerse the scaffolds twice in 96 % ethanol. Finally, the degree of cell adhesion and proliferation was assessed by scanning electron microscopy (SEM). The scaffolds were analysed after sputtering the materials with gold, using a JEOL JSM-7500F microscope (JEOL Ltd., Tokyo, Japan). *Statistical analysis:* One-way analyses of variance (ANOVA) were performed to demonstrate statistically significant differences between the two groups of results. The differences obtained were considered statistically significant at probabilities of $^{*}p < 0.05$, $^{**}p < 0.01$, $^{***}p < 0.001$ (Origin Pro 2019 Software, Originlab, MA, USA).

3. Results

3.1. Optimisation of the reaction conditions

This work presents the possibility of constructing dressing materials using a representative of the group of biodegradable and biocompatible PHAs, P(3HO). Fig. 1A provides a flow diagram of the P(3HO) preparation used in this work. Further, the solvent-free reaction of the simultaneous modification and decomposition of P(3HO) was used to obtain Dic-oligo(3HAs) is also presented. In this work, *p*-TSA was used as a catalyst/hydrolysing agent. The experiments involved a series of reactions using different reaction temperatures and varying amounts of reagents (DIC and *p*-TSA). To terminate the reaction, the post-reaction mixture was cooled and then dissolved in chloroform; washed with an aqueous solution of sodium chloride, as well as water, and precipitated in cold methanol. DIC is a substance with good solubility in both chloroform and methanol; however, it is poorly soluble in water. Therefore, no unreacted substrate was removed during the extraction step of the reaction mixture with aqueous sodium chloride solution and water. The confirmation of which signals originated from the introduced DIC was obtained by an experiment in which, after ^{1}H NMR analysis of the reaction mixture (Fig. 1B-C), a second spectrum measurement was made for an identical sample, after the addition of five drops of DIC solution (25 g•L^{-1}) [25]. The **H8** signal was associated with the protons of the DIC's methylene unit, which are adjacent to the ester group that links the active substance to the oligomers of the 3-hydroxyalkanoic acids (3HAs). To enable the analysis of the samples characterised by high molecular weights, based on the knowledge that low-molecular-weight P(3HO) fractions (oligomers below 2000 Da) are soluble in alcohols (e.g., methanol), the final reaction mixtures were precipitated after a extraction step. Subsequently, the precipitated fractions – characterised by a higher molecular weight and the fractions obtained after evaporation of the methanol used for precipitation were subjected to ^{1}H NMR analyses. Further, ^{1}H NMR analyses of all the precipitated fractions were carried out. For analyses of products obtained at 65 °C and 85 °C, only signals from unmodified oligomers and free, unbound DIC are noticeable (**H8'**, Fig. S1). In the case of the precipitated parts of the reaction mixtures obtained during the reactions conducted at higher temperatures (105 °C and 125 °C) (Fig. S2), the appearance of a new signal ($\delta = 3.78$ ppm) was observed (**H8**). The amount of attached compound in the precipitated part of the reaction mixture ranged from 0 to 27%mol. of DIC (Fig. 1E). Furthermore, the ^{1}H NMR analyses of all the methanol fractions confirmed the heterogeneity of the mixture, which also includes linear unmodified oligomers of 3-hydroxycarboxylic acids, physically bound DIC, and Dic-oligo(3HAs) (Fig. S3). The amount of attached DIC in the methanol fraction of the reaction mixture ranged from 6.4 to 64.2%mol. of DIC (Fig. 1D).

3.2. The spectroscopic analysis of Dic-oligo(3HAs)

Fig. S4 presents an analysis of the COSY spectrum, making it possible to assign the precise δ at which they appear to specific protons (Table S1). Afterwards, the HSQC analysis allowed correlation of the δ at which the signals from protons were read in the previous section with the corresponding δ of the carbon atoms (Fig. S5). Based on these results, the ^{13}C NMR spectrum was analysed, together with the assignment of carbon atoms to the specific δ where the signals were read (Figs. S6–7). Further, the HMBC analysis demonstrated the correlation of signals attributed to hydrogen atoms with signals from carbon atoms that were at least three bonds away from it. By using HMBC analysis, it was confirmed that the signal at $\delta = 3.78$ ppm recorded in the ^{1}H NMR measurements correspond to the protons (**H8**) of the methylene group of DIC, which is directly adjacent to the ester bond connecting the active substance to the oligo(3HAs)− a correlation between H9 and C14 (Fig. S8). Taking the above into account, it can be summarised that the introduction of an additional purification step, via extraction of the reaction mixture with an aqueous NaOH solution, enabled the conversion of unreacted DIC to its sodium salt, which has excellent solubility in water. Data on the solubility of diclofenac sodium in water vary, depending on the source, database or sales brochures. Nevertheless, the solubility is always >20 mg•mL^{-1}. Leaching out the resulting diclofenac sodium salt from the reaction mixture resulted in a product that contains only unmodified oligo(3HAs) and Dic-oligo(3HAs). Subsequently, the resulting reaction mixture was analysed by mass spectrometry using electrospray ionisation (ESI-MS). Fig. S9 shows an ESI-MS spectrum of Dic-oligo(3HAs) performed in positive ionisation mode, which made it possible to confirm the structures of the compounds composing the reaction mixture.

3.3. The release of DIC and DIC/3HAs and their kinetic models

The release profiles of DIC from Dic-oligo(3HAs) were determined using ^{1}H NMR. The use of ^{1}H NMR made it possible to record changes in the area under the signal at $\delta = 3.75$ ppm, which were attributed to the methylene groups of DIC in Dic-oligo(3HAs) (Fig. S11A). This indicates that during the measurements it was possible to record the release of DIC, its esters (DIC/3HAs), or its oligomeric forms (dimers, trimmers, or molecules characterised by higher molecular weight) (Fig. S11B). For the experiments conducted in D_2O, in the 1st hour, the release of 7.7% mol. of DIC or DIC/3HAs was recorded (Fig. S11C). In the following hours, the active substances were gradually released. After 48 h of ongoing release in D_2O, 82.08%mol of DIC or DIC/3HAs were determined. Otherwise, when a phosphate buffer at pH 7.4 and 5.0 was used as the incubation medium, the release profiles of the active substances were different (Fig. S11C). Within the 1st hour of the process carried out at pH 7.4 and 5.0, rapid release of DIC was recorded, at 74.35%mol. and 68.50%mol., respectively. The almost complete release of all the active substances encapsulated in the polymeric carrier was recorded within 12 h. The DIC released at the 12th hour when the material was incubated at pH 7.4 and 5.0 was 93.57%mol. and 93.90%mol., respectively. This phenomenon was related to DIC's solubility, which varies depending on the medium used. The solubility of DIC in water is about 77 times lower (17.8 mg•L^{-1}) than the solubility of this compound in PBS at pH 7.4 (1.37 g•L^{-1}) [28,29].

The results obtained from the release experiments were used to simulate Higuchi, Hixson and Korsmeyer-Peppas kinetic models. The highest correlation coefficient obtained (R^2) indicates which kinetic model is most suitable to describe the release of DIC, or DIC/3HAs [30]. The release of DIC, or DIC/3HAs into a control medium (D_2O) is best described by a Hixon model. When PBS was used as the medium in which the release processes of DIC and DIC/3HAs were simulated, irrespective of the pH of the medium, the results indicate that the Korsmeyer-Peppas model is the most appropriate (Table S3.). An important parameter describing the release mechanism according to

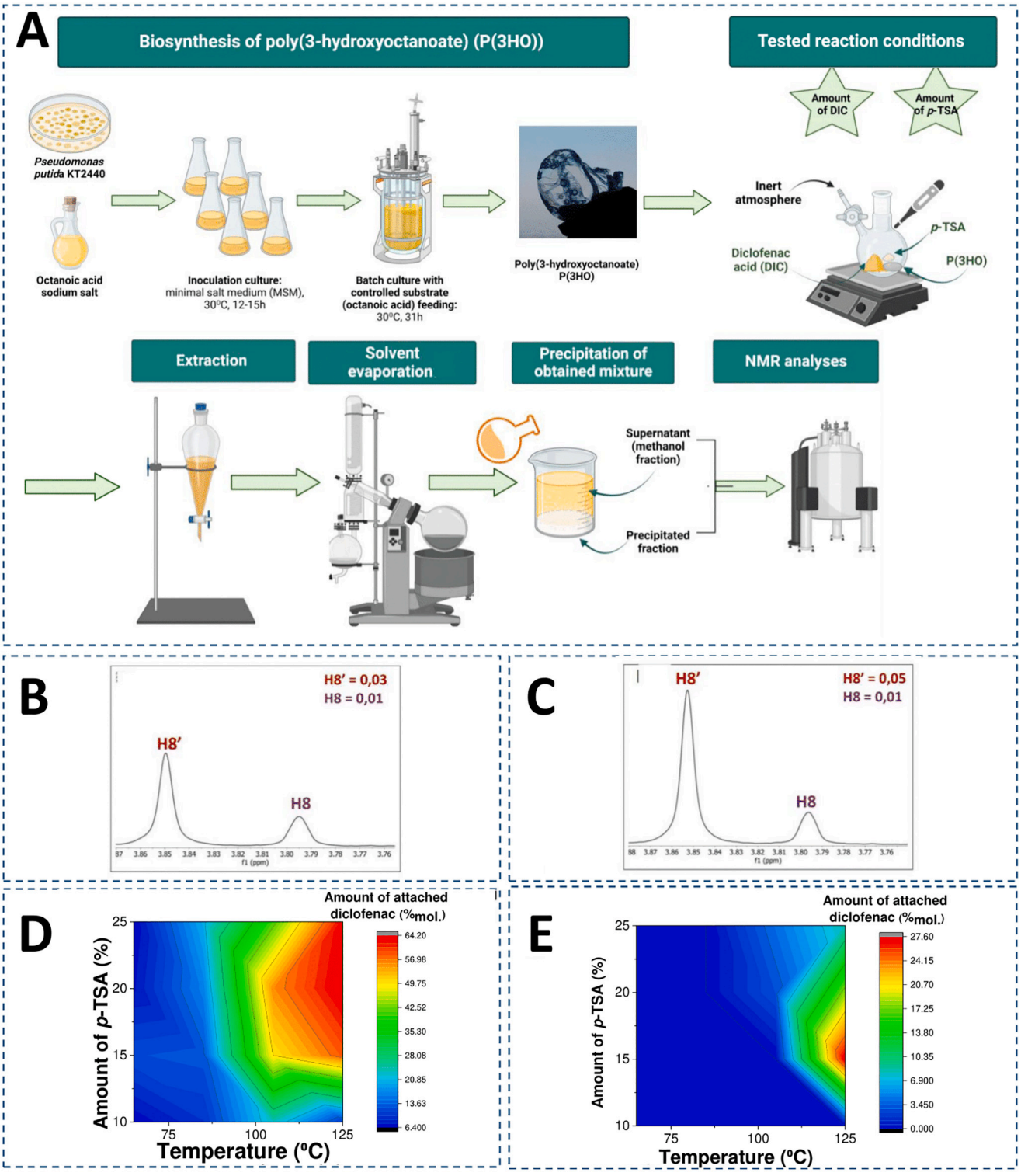

Fig. 1. **(A)** A scheme of the experimental pathway leading to the preparation of Dic-oligo(3HAs). The processing included biosynthesis of the bacterial polymer P(3HO), testing the reaction parameters, post-synthetic treatment of the resulting reaction mixtures, as well as NMR analyses. Created with BioRender.com; **(B)** ^{1}H NMR of the Dic-oligo(3HAs) reaction mixture; **(C)** an identical sample after addition of four drops of diclofenac solution (25 g·L^{-1}). As **H8** are the protons of the –CH2– group of DIC adjacent to the ester linkage between the active substance and the 3HAs oligomers, **H8'** are the atoms of the protons of the –CH2– of DIC; **(D)** The surface response graph showing the %mol. of DIC attached via covalent bonding to 3HAs in the methanol part of the reaction mixtures. The plot shows the variation in the amount of DIC attached to 3HAs as a function of the amount of *p*-TSA used and the reaction temperature; **(E)** Parallel plot showing the variation obtained in the precipitation parts of the reaction mixtures.

Korsmeyer-Peppas kinetics is the exponent n, which indicates by which mechanism the active substances are released. When PBS at pH 7.4 was used as the reaction medium, the value of n was 0.524 ($0.5 < n < 1$), indicating anomalous diffusion taking place without obeying Fick's laws of diffusion (coupling of diffusion and erosion of the polymer carrier) [31]. When PBS at pH 5.0 was used as the medium, the exponent n was 0.411 ($0.30 < n < 0.45$). This result indicates that, the release of the substance is controlled by diffusion according to Fick's laws. In the first hour, there was a rapid release of active substances due to differences in the concentrations of the bioactive substances in the medium and the polymer carrier [32]. Thereafter, a gradual and steady release of the remaining substances in the carrier was observed. The parameters of the release constant (K) are determined to be the same for the release processes carried out at both pH 7.4 and pH 5.0. Considering this, it can be concluded that the release of substances from these carriers does not depend on the pH, but on the diffusion laws governing this process [33].

3.4. Physicochemical properties of the Dic-oligo(3HAs)

The wettability of films prepared using the P(3HO)/Dic-oligo(3HAs) blend was assessed using the sitting drop method. The wettability values for the liquids, which were polar water and non-polar diiodomethane, were 108 ± 2^0 and 65 ± 2^0, respectively (Fig. S12). The surface free energy characterising P(3HO)/Dic-oligo(3HAs) was determined based on the results obtained in the experiment described above. The values of the polar, dispersive and summed surface energy for P(3HO)/Dic-oligo (3HAs) were 23.51 ± 0.25 mN•m^{-1}; 3.87 ± 0.16 mN•m^{-1} and 26.34 ± 0.45 mN•m^{-1}, respectively (Fig. S13).

3.5. Structural analysis of the prepared patches

The porous wound dressings were obtained using an SCPL technique (Fig. 2A). The μ-CT photographs show three-dimensional models, interconnected pores (Fig. 2B) and reconstructed cross-sections (Fig. S14). All the materials obtained were characterised by a high degree of open porosity (> 72 %), with a low proportion of closed porosity (< 0.2 %) (Table 2). Among the two groups of materials, (1) constructed from P(3HO) and (2) P(3HO)/Dic-oligo(3HAs)) prepared using the ratio of 5 % P(3HO)/95 % NaCl had the highest degree of porosity, which was 76.20 % and 83.70 % for 5P(3HO) and 5P(3HO)/Dic-oligo(3HAs),

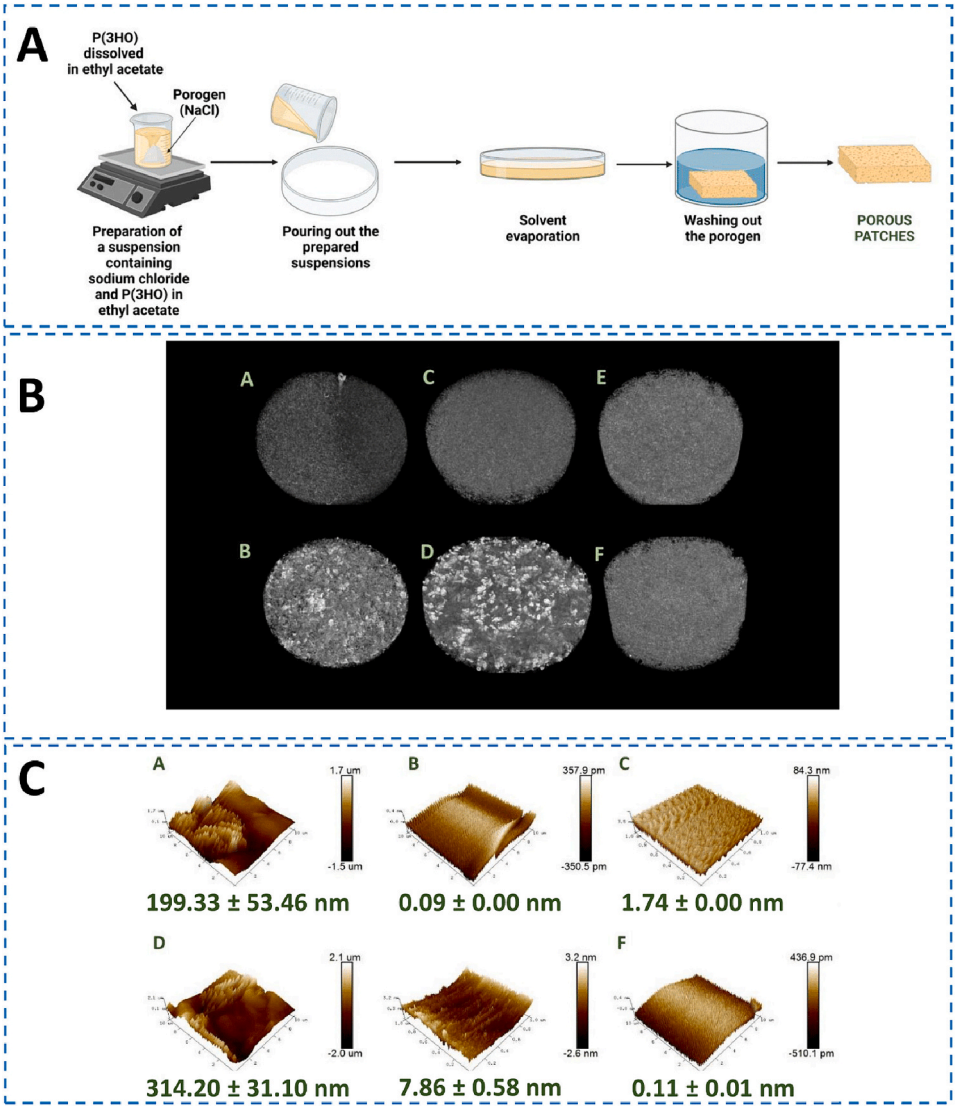

Fig. 2. **(A)** Demonstration of the preparation of porous patches. Created with BioRender.com; **(B)** Three-dimensional reconstructed models of the prepared patches: (a) 5P(3HO); (b) 5(P3HO)/Dic-oligo(3HAs); (c) 15P(3HO); (d) 15P(3HO)/Dic-oligo(3HAs); (e) 25P(3HO); (f) 25P(3HO)/Dic-oligo(3HAs); **(C)** Topographical images of the prepared patches and the roughness determined for each: (a) 5P(3HO); (b) 5(P3HO)/Dic-oligo(3HAs); (c) 15P(3HO); (d) 15P(3HO)/Dic-oligo(3HAs); (e) 25P (3HO); (f) 25P(3HO)/Dic-oligo(3HAs).

Table 2
The degree of porosity of the prepared materials.

	Open porosity (%)	Closed porosity (%)	Total porosity (%)
5P(3HO)	76.20	0.00	76.20
5P(3HO)/Dic-oligo (3HAs)	83.70	0.07	83.77
15P(3HO)	73.30	0.06	73.36
15P(3HO)/Dic-oligo (3HAs)	76.70	0.15	76.85
25P(3HO)	76.00	0.07	76.07
25P(3HO)/Dic-oligo (3HAs)	72.20	0.14	72.34

respectively (Table 2). Fig. S15 shows that the analyses revealed a large population of pores with a diameter of <100 μm, which is inconsistent with the diameter of the porogen grains used. However, the smaller pores may have been formed during one of the material preparation steps (mixing the porogen grains with the polymer solution).

Projections of the three-dimensional topographic regions of the prepared patches were obtained by AFM analyses (Fig. 2C). Heterogeneous patterns and the presence of elongated structures characterise all the imaged surface topographies. The highest roughness values were recorded for materials prepared using the highest amount of porogen (95 % NaCl, for both P(3HO) and P(3HO)/Dic-oligo(3HAs). The roughness for 5P(3HO) and 5P(3HO)/Dic-oligo(3HAs) was 193.33 ± 53.46 nm and 314.20 ± 31.10 nm, respectively. For materials made from blends supplemented with Dic-oligo(3HAs), the surface roughness of the patches decreased with increasing amounts of polymer used. When the patches were prepared using the ratio of the reagents: 85 % NaCl/15 % P(3HO), the roughness of the 15P(3HO)/Dic-oligo(3HAs) was 7.86 ± 0.58 nm. Subsequently, for patches prepared with 75 % NaCl and 25 % P(3HO), the roughness of 25P(3HO)/Dic-oligo(3HAs) was 0.11 ± 0.01 nm. In contrast, for patches made from P(3HO), no apparent decreasing trend in roughness with increasing amounts of P (3HO) used in the preparation was observed. The roughness of the 15P (3HO) and 25P(3HO) was 0.09 ± 0.00 nm and 1.74 ± 0.00 nm, respectively.

Next, the basic mechanical parameters of the prepared patches were determined (Figs. S16). In the case of dressings, it is desirable that the material is flexible and has a high tensile strength and a correspondingly high elongation at break. Our analysis showed that Young's modulus increased as the amount of polymer used increased. The Young's modulus for 5P(3HO), 15(3HO) and 25P(3HO) were 1.07 ± 0.49 MPa, 0.95 ± 0.41 MPa and 2.72 ± 0.61 MPa, respectively. Additionally, similar relationships were recorded for tensile strength and elongation at break. The highest values were recorded for 25P(3HO), which were 0.83 ± 0.12 MPa and 127.56 ± 10.60 %, respectively. Considering that it is important that the dressing material is sufficiently flexible and can be deformed, the 25P(3HO) material is not suitable for wound treatment. Surprisingly, it was observed in all cases that adding Dic-oligo (3HAs) increased the Young's modulus, tensile strength and elongation at break. Furthermore, no statistically significant differences were shown for the Young's modulus, tensile strength and elongation at break for 5P(3HO)/Dic-oligo(3HAs) and 15P(3HO)/Dic-oligo(3HAs).

3.6. Biological assays on prepared materials

To determine the ability to inhibit the growth of microorganisms of the synthesised Dic-oligo(3HAs), minimum inhibitory concentrations (MIC_{90}) were determined using the microdilution method. Our findings indicate a varied susceptibility of Gram-positive bacteria to diclofenac with MIC_{90} ranging between 50 and 100 $\mu g \cdot mL^{-1}$. Specifically, strains such as *S. aureus* (ATCC 65p) and *S. epidermidis* (RP62a) are less susceptible to DIC, exhibiting MIC_{90} at the higher end of the spectrum (100 $\mu g \cdot mL^{-1}$). Conversely, *S. aureus* ATCC 29213 and *E. faecalis* ATCC 29212 demonstrated greater susceptibility, as reflected by lower MIC_{90} (50 $\mu g \cdot mL^{-1}$) (Table 3).

Further, we conducted also a comparative analysis of the antimicrobial effects of DIC and Dic-oligo(3HAs) on clinical strains of *Staphylococcus* spp., focusing on their ability to inhibit bacterial growth at various concentrations. The investigation, illustrated through growth curves in Fig. 3, revealed that both compounds exert a concentration-dependent inhibitory effect on bacterial proliferation. Notably, Dic-oligo(3HAs) demonstrated a markedly higher potency, inhibiting bacterial growth at significantly lower concentrations compared to diclofenac. At the highest tested concentrations, both compounds induced a delay in the bacterial growth phases, yet the impact was more pronounced with Dic-oligo(3HAs). This difference in efficacy suggests that Dic-oligo(3HAs) interacts with bacterial cells more effectively, potentially due to a higher affinity to cell walls or enhanced cellular uptake, which needs further investigation.

Indirect cytotoxicity tests were performed to evaluate the toxicity of the prepared materials. The experiments were carried out according to ISO 10993-5, in which extracts were tested after 24 h of incubation of the materials in culture medium (DMEM). HaCaT were incubated for 24 h in the resulting extract, and the cytotoxicity was then assessed using two techniques: (1) quantitative, which was based on resazurin reduction; (2) qualitative, by staining live cells with calcein green AM as well as dead cells with propidium iodide. The quantitative tests (Fig. 4A) showed cell viability after 24 h of exposure to the obtained extracts was higher than 90 %, compared to the negative control. A higher viability, compared to the negative control, was observed for 5P(3HO), 5P(3HO)/Dic-oligo(3HAs) and 15P(3HO). This is related to the nutritional properties of (*R*)-3-hydroxycarboxylic acids, which are released during the incubation of the materials [24]. The slightly lower viability observed for the 15P(3HO)/Dic-oligo(3HAs), 25P(3HO) and 25P(3HO)/Dic-oligo (3HAs) may be related to the leaching of the non-leached salt that played the role of porogen during the preparation of the porous materials. The results of the qualitative analysis performed using a fluorescence microscope after staining the cells with calcein green AM and propidium iodide, are shown in Fig. 4B. A large number of living cells, as well as the absence of dead cells were observed. This confirms the absence of cytotoxicity, which is consistent with the results of the spectrophotometric tests.

Next, direct cytotoxicity assays were performed, in which HaCaT were cultured for two days directly on the surfaces of the test materials. After this, the HaCaT were stained with calcein green AM and propidium iodide, after which they were visualised by confocal microscopy (Fig. 4C). In the Fig. 4C shown, viable cells with a spherical shape and a tendency to form clusters were observed. The highest number of viable cells, similar to the number observed for the negative control, a polystyrene surface, were observed for materials: 5P(3HO), 5P(3HO)/Dic-oligo(3HAs) and 15P(3HO). This may indicate a similar adhesion of HaCaT to the surface of these materials.

The direct proliferation analysis showed an increase in the number of HaCaT during culture on biomaterials: 5P(3HO), 5P(3HO)/Dic-oligo (3HAs) and 15P(3HO) (Fig. 5A). This indicates that the properties of

Table 3
Comparison of MIC_{90} for Dic and Dic-oligo(3HAs).

Bacteria strain	MIC_{90} ($\mu g \cdot mL^{-1}$)	
	DIC	Dic-oligo(3Has)
S. aureus ATCC 6538p	100	5
S. aureus ATCC 29213	50	5
S. epidermidis RP62a	100	10
E. faecalis ATCC 29212	50	10
E. coli NCTC10538	nd	nd
K. pneumoniae ATCC 10031	nd	nd
P. aeruginosa ATCC 27853	nd	nd

nd – not detected.

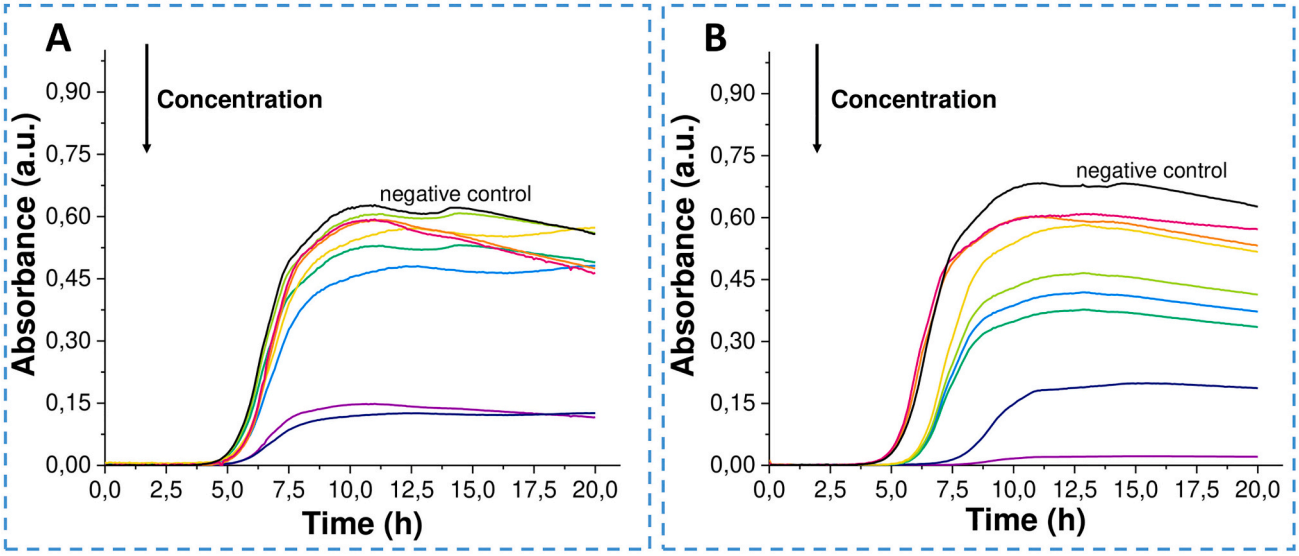

Fig. 3. Presentation of the growth of clinical *Staphylococcal* isolates **(A)** O–121 and **(B)** O–202 over time at different concentrations of Dic-oligo(3HAs). With increasing concentrations of Dic-oligo(3HAs), lower OD values were registered, as shown by the arrow in the graphs. The negative control (oligo-3HAs) is shown as a black curve.

the patches favour HaCaT proliferation on their surface. In the case of the other materials [15P(3HO)/Dic-oligo(3HAs), 25P(3HO) and 25P (3HO)/Dic-oligo(3HAs)], a decrease in the number of cells was observed on the 11th day, compared to the 7th day of the conducted experiment (Fig. S17). This indicates that some cells died and/or ceased cell division. Based on the results shown in Fig. 5A, the rate of cell proliferation on the scaffolds was calculated (Fig. S18). The analyses showed there were no statistically significant differences in the cell proliferation rates on the surfaces of the 5P(3HO) ($0.017 \pm 0.002\ h^{-1}$), 15P(3HO) ($0.013 \pm 0.000\ h^{-1}$) and 5P(3HO)/Dic-oligo(3HAs) ($0.018 \pm 0.002\ h^{-1}$). When HaCaT were cultured on the surface of the other biomaterials, significantly lower cell population proliferation rates were observed. These were $0.005 \pm 0.002\ h^{-1}$, $0.009 \pm 0.003\ h^{-1}$ and $0.006 \pm 0.003\ h^{-1}$ for 25P(3HO), 15P(3HO)/Dic-oligo(3HAs) and 25P(3HO)/Dic-oligo(3HAs), respectively.

The HaCaT present on the scaffolds on the 14th day of the experiment were visualised using confocal microscopy after being stained with calcein green AM and propidium iodide (Fig. 5B). The highest number of viable cells was observed for 5P(3HO), 5P(3HO)/Dic-oligo(3HAs) and 15P(3HO). The study showed parallelism for the results obtained from the analyses of the materials [15P(3HO)/Dic-oligo(3HAs), 25P(3HO) and 25P(3HO)/Dic-oligo(3HAs)]. Single live and dead cells were observed on their surface. Only the few dead cells observed on the surface of these scaffolds may be caused by the washing of the materials while preparing the cell stains.

Taking into account the fact that only materials prepared using a ratio of 5 % P(3HO) or P(3HO)/Dic-oligo(3HAs) and 95 % NaCl were characterised by a lack of cytotoxicity, as well as biocompatibility confirmed via HaCaT proliferation assays; the next stage of the work focuses on the analyses of 5P(3HO) and 5P(3HO)/Dic-oligo(3HAs). Following this, analyses were performed to demonstrate that HaCaT penetrate deep into the prepared materials. To graphically represent this, cell nuclei were stained with DAPI dye and observed using confocal microscopy (Fig. 6A–B). The three-dimensional graphs demonstrate that HaCaT colonise the surface similarly deep into the material. For the 5P (3HO) and 5P(3HO)/Dic-oligo(3HAs) materials, this is 295 μm and 275 μm, respectively. To demonstrate how the cells behave during cultivation, the cytoskeleton of the cells was further stained with phalloidin-TRITC (Fig. 6I–K). It can be observed that the cells colonise biomaterials primarily by adhering to their pores. In addition, through SEM analyses, it was presented that HaCaT not only colonise biomaterials deeply but also grow on their surface (Fig. 6C–H). Furthermore, the presence of NaCl residues was observed in photographs showing the surface of 5P(3HO). The observation indicating ineffective leaching of NaCl from biomaterials has already been noted for μ-CT analyses.

4. Discussion

4.1. Dic-oligo(3HAs) as a component of dressing materials

This paper presents the characterisation of P(3HO) and P(3HO)-based porous patches supplemented with Dic-oligo(3HAs). The biomaterials produced are promising materials for applications in skin regeneration processes. This is because topical delivery of active substances makes it possible to increase the bioavailability of drugs and, above all, to prevent several side effects associated with the oral intake of drugs [34]. The stratum corneum is a selective barrier to drug penetration. To allow topical delivery of hydrophobic drugs to the deeper layers of the skin, compounds are used that improve penetration. Such molecules include fatty acids, polyalcohols or surfactants [35]. As shown in the mass spectrometry (MS) analysis, in the filtrate obtained from precipitation of the post-reaction mixture, which mimics the conditions under which DIC can be released, the presence of free unbound DIC, with a molecular weight of 295 Da, was not recorded. In contrast, its conjugates with hydroxyl derivatives of fatty acids, which have a molecular weight of 578 Da, were observed. The MS analysis showed that the reaction mixture contained different chain-length cyclic hydroxy fatty acid derivatives (Fig. S9). The release of active substances from polymeric drug carriers is linked to various physical and chemical processes: dissolution, permeation, diffusion or erosion [30]. The release profile of the active substance also depends on the physicochemical properties of the polymer carrier, including its chemical structure and dimensions. Herein, the release experiments of the active substance (Fig. S11C) were conducted using low-molecular-weight DIC carriers. One can assume that, in the case of releasing active substances from a blend prepared for the preparation of patches, the delivery of DIC, or DIC/3HAs, to a well-defined site will be prolonged.

The study of drug release kinetic models is an important step in predicting the behaviour of prepared formulations in contact with a living organism in vivo. The kinetics of drug release are influenced by a number of parameters that include the pH present at the application site, drug solubility, as well as various other physiological parameters [36].

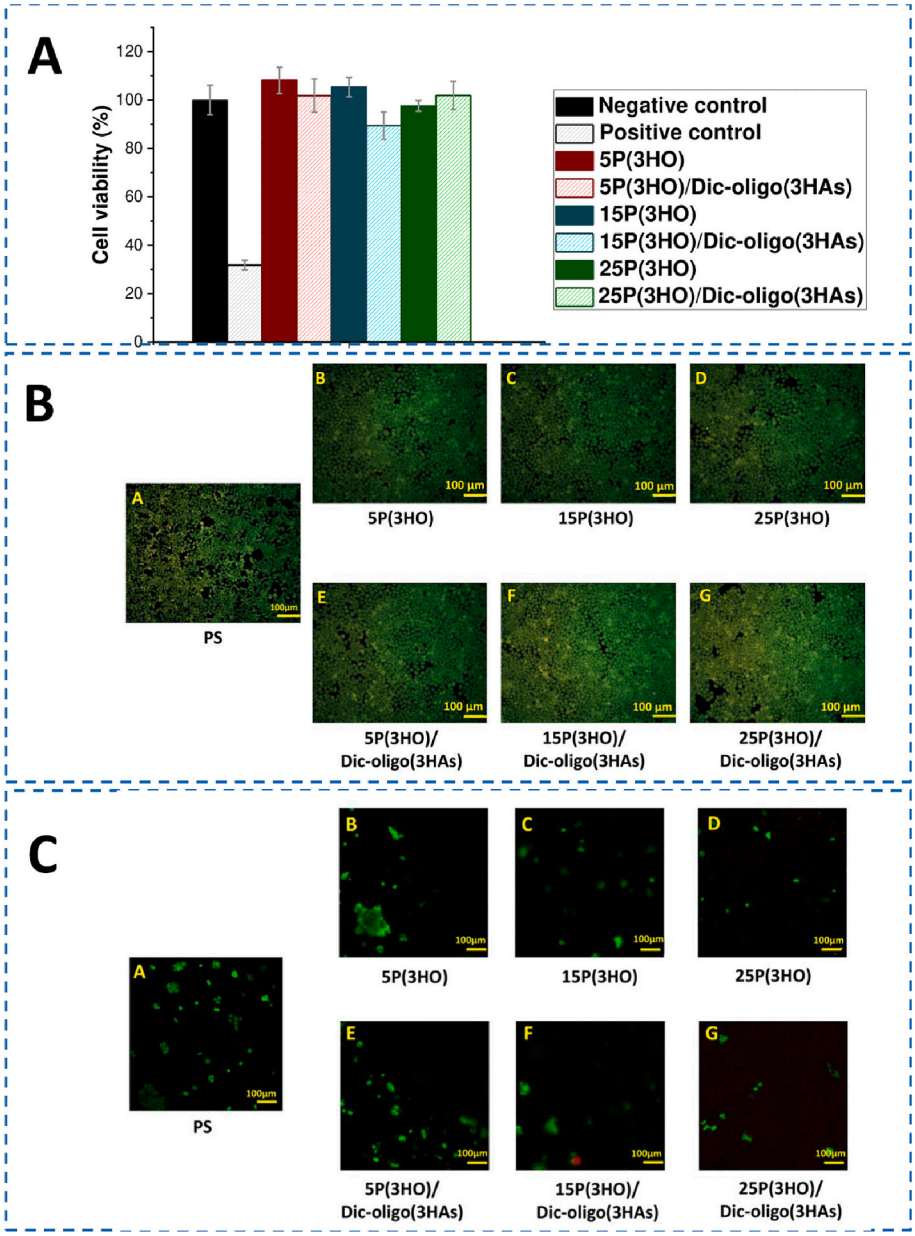

Fig. 4. **(A)** The indirect cytotoxicity of the prepared materials determined in a spectrophotometric test (n = 3, N = 3); **(B)** The Live/Dead assay performed after indirect analysis in which cells were incubated in the presence of extracts derived from biomaterial incubation in DMEM; **(C)** The direct cytotoxicity assay assessed by Live/Dead staining (n = 3, N = 3).

The kinetic models presented in this study showed that at pH 7.4 and 5.0, they are released from the prepared carriers according to the Korsmeyer-Peppas mechanism (Table S3). According to the assumptions of this model, the release of the active substances was shown to follow a passive mechanism. The analysis presented here shows that the release of active substances is not dependent on the pH of the environment. Taking this into account, the active substances should be released in a similar manner, both for applications in the treatment of chronic skin wounds (pH = 5.0) and normally healing wounds (pH = 7.4).

Herein, a representative of mcl-PHA, to construct the dressing carriers of active substances was used. P(3HO) comprises repeating units of hydroxylated fatty acid derivatives. As is well known, fatty acids are involved in the metabolism of processes occurring during or following inflammation (e.g., blood vessel contraction, cell adhesion and death, or tissue regeneration) [37]. The concentration of 100 μg Dic-oligo(3HAs)/1 g P(3HO) used in this study is an amount that should have a therapeutic effect while limiting the toxic effect of the substance on regenerated tissues. As shown in a study presented by Sioufi et al., the minimum therapeutic concentration of DIC (IC_{50}) that was able to inhibit 50 % prostaglandin (PGE2) synthesis in synovial fluid was 45 ng•mL^{-1} [38]. Ex vivo studies using a gel containing DIC (Emulgel 1 %) showed that 12.5 ± 3.2 % (~1.25 mg) of the applied drug is absorbed in the skin [39]. Additionally, using three-dimensional patches as topical delivery systems for DIC in regenerated skin is promising. As shown in a study prepared by Haltner-Ukomadu et al., the use of a three-dimensional hydrogel as a carrier for DIC in the topical delivery of the drug increased its permeability through the skin by 280 %, compared to Emulgel 1 % [39]. Numerous literature reports demonstrate the supportive effects of fatty acids, for example, linoleic acid, α-linolenic acid, or oleic acid, in the regeneration of chronic skin wounds [37]. In the work presented by Mohanty et al., in vivo studies were conducted on dressings containing oleic acid and curcumin [40]. The authors showed that using these dressings improved the wound-healing process compared to the control material. These observations were supported by

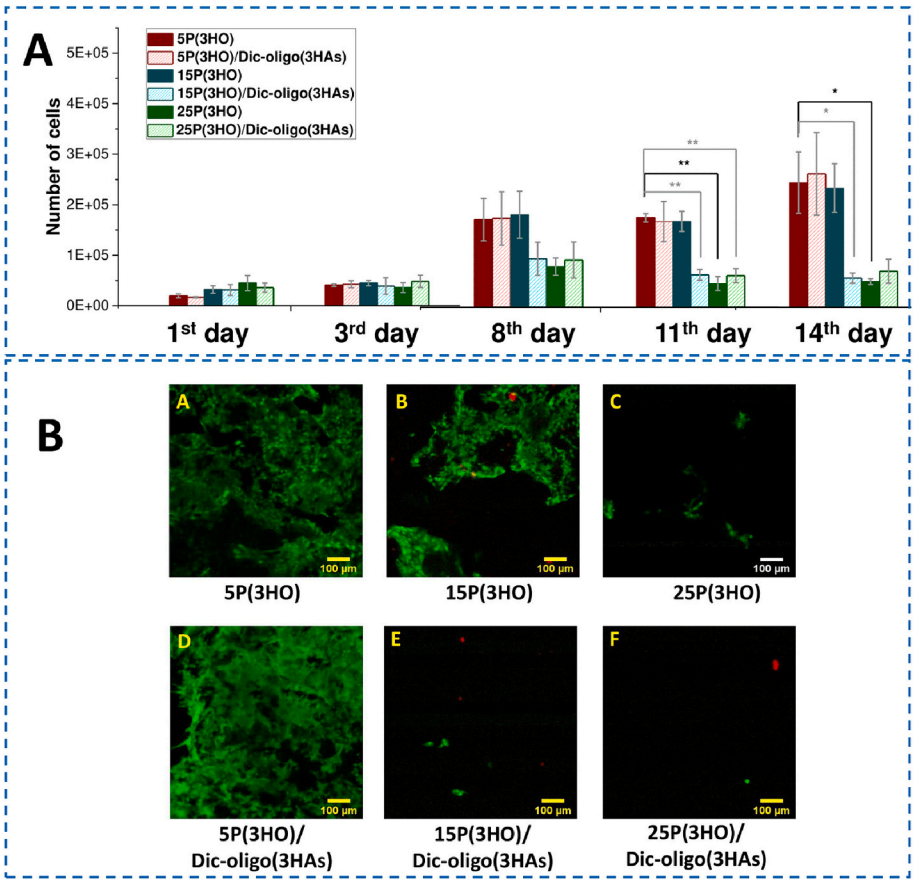

Fig. 5. **(A)** The direct HaCaT proliferation test performed on the scaffold surface shows the increase in the number of cells over the experiment (n = 3, N = 3). The results are statistically significant when: *p < 0.05, **p < 0.01, and ***p < 0.001; **(B)** The analysis of direct HaCaT proliferation on biomaterial surfaces on day 14 of the conducted experiment, evaluated by Live/Dead staining assays.

curcumin inhibiting further inflammation at the wound site due to its anti-inflammatory properties. Furthermore, the authors hypothesised that oleic acid ensures the sustained release of curcumin and its better bioavailability due to the solubility of its metabolites (sulphates or glucoronates) in fatty acids [40].

4.2. *Correlation of the structural properties of patches with their in vitro biological characteristics*

The interactions between eukaryotic and prokaryotic cells and the dressing material depend on their surface parameters, including wettability, surface energy, and roughness [41]. Wettability is an important parameter determining eukaryotic cells behaviour, bacterial adhesion, and protein adsorption. P(3HO) and P(3HO)/Dic-oligo(3HAs) are hydrophobic. The wettability for these materials is 108 ± 2^0 and 100 ± 1^0, respectively. As is known from literature data, the hydrophobicity of material surfaces affects the adhesion of *Staphylococcus aureus*, a pathogen that colonises the skin and has great pathogenic potential. The bacterial infection caused by *S. aureus* is particularly difficult to treat due to this pathogen's extensive antibiotic resistance. As was shown, *S. aureus* creates a denser biofilm on hydrophilic surfaces. It is known that the virulence of bacterial strains is closely related to the density of the bacterial film formed [42]. Considering the above, using hydrophobic P(3HO) to construct wound patches should reduce the possibility of pathogen adhesion, especially of the *S. aureus* species. This is particularly relevant when using such materials in treating chronic skin wounds, including, among others, diabetic wounds, which have a limited ability to regenerate [43]. The active ingredient used in this work, diclofenac, is also worthy of attention in terms of its antimicrobial activity. In the literature data, there is information that it has an inhibitory effect on various virulence factors of methicillin-resistant *S. aureus*, including biofilm formation [44]. Ferrer-Luque et al. postulated that the mechanism of diclofenac's antimicrobial action may be linked to inhibition of microbial cell wall synthesis, alteration of membrane damage, and inhibition of nucleic acid synthesis [45]. Ullah et al. presented approaches for the fabrication of electrospun nanofibers made from soy protein, hydroxyethylcellulose and halloysite nanotubes, which were subsided by the addition of diclofenac sodium. The samples were prepared for wound healing applications. The study demonstrated antimicrobial efficacy against *E. coli* and *B. subtilis* strains, which was provided just by the addition of diclofenac sodium [46].

Having the above in mind we have performed preliminary assessment of the new P(3HO) bioadditives and assessed their biological action against a panel of bacteria (Table 3). This variability underscores the selective efficacy of DIC across different Gram-positive bacterial strains. In contrast, Dic-oligo(3HAs) exhibits remarkably higher antimicrobial potency against the same Gram-positive strains, with MIC_{90} significantly lower than those observed for DIC, ranging from 5 to 10 $\mu g \cdot mL^{-1}$. This stark contrast in efficacy not only highlights the superior antimicrobial properties of Dic-oligo(3HAs) but also its potential as a more effective therapeutic option against Gram-positive bacterial infections. Notably, our analysis extends to Gram-negative bacteria, where both DIC and Dic-oligo(3HAs) demonstrated no discernible activity, with MIC values potentially exceeding 800 $\mu g \cdot mL^{-1}$. This lack of efficacy indicates a resistance mechanism inherent to Gram-negative bacteria, possibly attributed to their unique cell wall composition that impedes the drugs' penetration, underscoring the challenge in developing broad-spectrum antimicrobials capable of targeting both Gram-

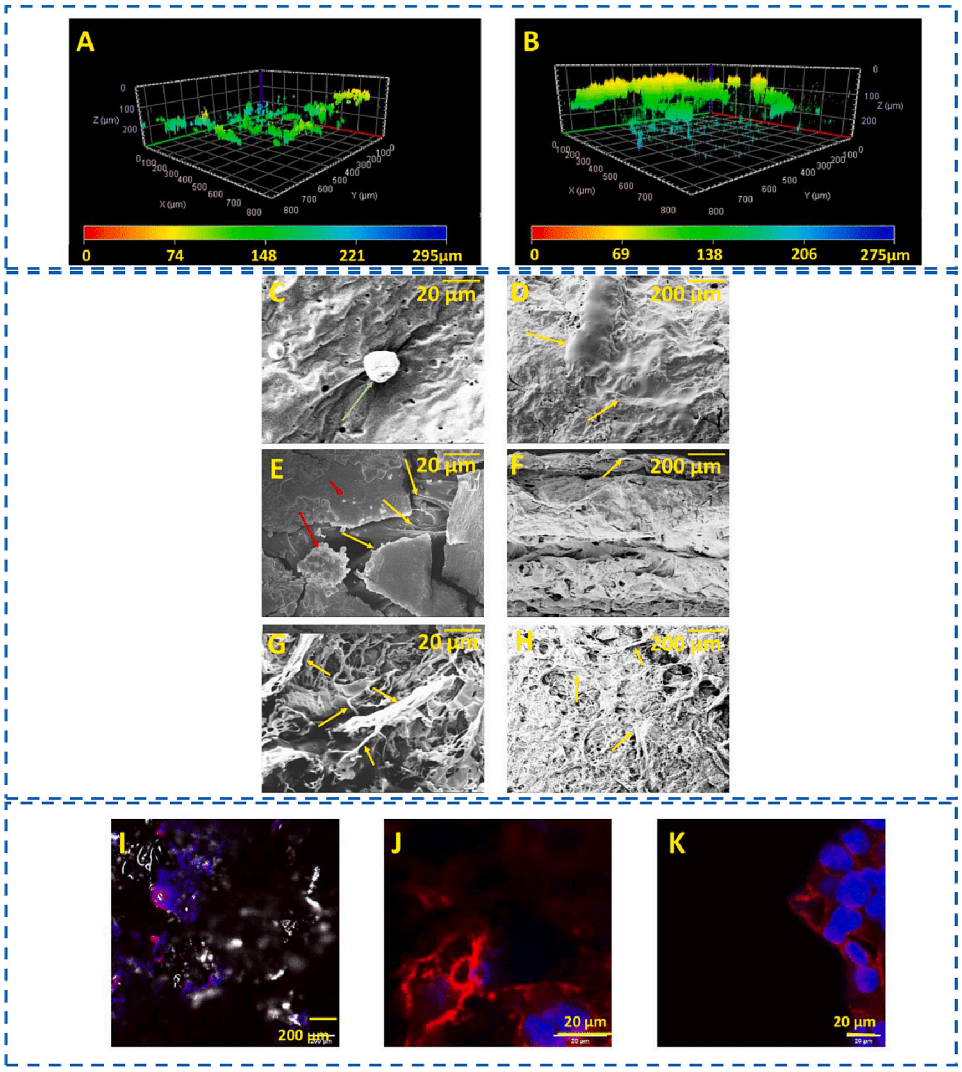

Fig. 6. The 3D reconstructions of the tested biomaterials showing the depth of cells penetration into the patches for **(A)** 5P(3HO) and **(B)** 5P(3HO)/Dic-oligo(3HAs); SEM microphotographs show **(C)** the surface of 5P(3HO) at day 1 of the proliferation assay; **(D)** the surface and **(E–F)** a cross-section of 5P(3HO) at day 14 of the proliferation assay; **(G–H)** the surface of 5P(3HO)/Dic-oligo(3Has)-Chem at day 14 of the proliferation assay. Yellow arrows indicate HaCaT, while red ones indicate unleached NaCl. The photographs presented in panels **I–K** show cells in the 5P(3HO) pores. The blue dye (DAPI) allowed staining of cell nuclei, while the red dye (phalloidin-TRITC) enabled observation of the cytoskeleton of the HaCaT.

positive and Gram-negative pathogens.

However, as shown in Fig. S12, the prepared blends containing 100 μg Dic-oligo(3HAs)/1 g P(3HO) have a 14^0 lower contact angle for water compared to P(3HO) [26]. Accordingly, HaCaT should preferentially adhere to P(3HO)/Dic-oligo(3HAs) materials. However, the microscopic observations presented in Fig. 4C show similar adhesion of HaCaT to materials made of both P(3HO) and P(3HO)/Dic-oligo(3HAs). In Fig. 4C, differences were observed that were not due to the addition of Dic-oligo (3HAs) but to the mass ratio of the reagents [P(3HO) and NaCl] used to prepare the porous materials. Skin is a hydrophobic tissue with surface energy values ranging from 25 to 29 $mN{\bullet}m^{-1}$. Liu described that materials for skin regeneration should have similar or lower surface energy values [47]. Taking the above into account, it can be concluded that P (3HO) and P(3HO)/Dic-oligo(3HAs) are good candidates for the construction of dressing materials because the surface energy for these materials was 7.22 ± 0.64 $mN{\bullet}m^{-1}$ and 26.34 ± 0.45 $mN{\bullet}m^{-1}$, respectively (Fig. S13).

An appropriate combination of a material's mechanical, physicochemical and structural properties influences the behaviour of cells (adhesion, proliferation and infiltration) on its surface [48]. The degree of porosity, pore size, and the mechanical properties of the materials are important parameters affecting the ability to simulate appropriate biomechanical properties that can mimic the extracellular matrix (ECM) of native tissue [49]. Commercially available dressing materials such as Smart Matrix® and Integra® are characterised by a highly porous structure (80–90 %) with a high proportion of open pores. The prepared patches had porosities of 72.20–83.70 % (Table 2). Among the patches, the group obtained using a mass ratio of 5 % P(3HO)/95 % NaCl was characterised as the one with the highest porosity, which was 76.20 % and 83.70 % for 5P(3HO) and 5P(3HO)/Dic-oligo(3HAs), respectively. The materials obtained were characterised by open porosity and different pore diameters (Fig. 2B). This is especially important because smaller pores transport nutrients and body fluids. In comparison, larger pores allow cells proliferation and infiltration [50]. The Young's modulus values for 5P(3HO) and 5P(3HO)/Dic-oligo(3HAs) were 1.07 ± 0.49 MPa and 2.09 ± 0.82 MPa, respectively, indicating that the materials were susceptible to elastic deformation (Fig. S16A). Moreover, these values were also in the range of the Young's modulus value which characterises human skin. Nevertheless, it should be noted that the Young's modulus values of the skin depend on the age of the patient from whom the tissue originated, the site of collection, and the measurement technique used. Considering the above, the range of values is

wide: 0.1–500.0 MPa [51]. The patches obtained in the present study were also characterised by high tensile strength and high elongation at break (Fig. S16B-C). The tensile strength for human skin (21.6 ± 8.4 MPa) is higher than these parameters for 5P(3HO) and 5P(3HO)/Dic-oligo(3HAs), which are 0.17 ± 0.02 MPa and 0.43 ± 0.11 MPa, respectively [52]. The values obtained for tensile strength and elongation at break demonstrate the flexibility of the prepared materials, making them suitable as a good barrier to protect wounds from the external environment.

Surface roughness is an important factor influencing cell adhesion and behaviour [49]. Materials with higher roughness should support eukaryotic cell adhesion more [48]. On the surface of materials with a higher roughness (Fig. 2C), more HaCaT were observed in the direct cytotoxicity tests (Fig. 4C). The initial degree of adhesion of HaCaT to the surface of the tested biomaterials tested also influenced the other results obtained in the bioassays. In addition to the ability of dermal cells to adhere to dressing materials, they should exhibit other properties that include biodegradability, bioactivity, biocompatibility, and the absence of cytotoxicity [53]. In this paper, the indirect cytotoxicity tests were performed in accordance with ISO 10993-5. These tests evaluated the toxicity of extracts after 24 h incubation of the prepared materials in DMEM. Figs. 4A–B show that the prepared materials are non-toxic to the HaCaT. Considering the above, the extracts from these materials should not cause an allergic reaction or irritation. NMR analyses (Figs. S4–S8) showed that the material is prepared from a polymer of repeating units of 3-hydroxycarboxylic acids. Furthermore, as is well known, fatty acids are natural metabolites found in human blood, which is important from a therapeutic perspective [27].

The wound healing process involves not only keratinocytes but also fibroblasts. Fibroblasts are responsible for processes related to the biosynthesis of the extracellular matrix (ECM) and the formation of new blood vessels. In turn, keratinocytes enable the reconstitution of the epidermis, which protects the underlying tissues from injury [54]. The possibility of HaCaT proliferation on the prepared biomaterials was evaluated in this study. Direct proliferation analysis performed using both the spectrophotometric (Fig. 5A) and the Live/Dead assay (Fig. 5B) showed that 5P(3HO) and 5P(3HO)/Dic-oligo(3HAs) promote HaCaT proliferation, both on their surface (Fig. 6C–H) and deep into their structure (Fig. 6A–B). The results presented here may provide a proof-of-concept for the biocompatibility of the biomaterials, as well as further commercialisation potential.

5. Conclusions

In this paper, the biomedical potentials of porous patches composed of P(3HO) and P(3HO) supplemented with Dic-oligo(3HAs) were confirmed. The conducted experiments showed that 5P(3HO) and 5P(3HO)/Dic-oligo(3HAs) materials exhibit sufficient surface energy, porosity, roughness and mechanical properties to allow HaCaT to adhere to their surface and further proliferate both on and into their structure. Moreover, synthesised Dic-oligo(3HAs) revealed antimicrobial activity against both – Gram-positive and Gram-negative pathogenic strains. Furthermore, the indirect cytotoxicity tests performed in accordance with ISO 10993-5 showed that the prepared patches are non-toxic to the HaCaT. Moreover, it was demonstrated that releasing active substances into the wound environment is not dependent on the pH. Therefore, it can be concluded that DIC will be released similarly in typically and severely healing wounds. This indicates the versatility of the prepared materials in the construction of wound dressing components, allowing the local delivery of DIC.

CRediT authorship contribution statement

Katarzyna Haraźna: Writing – review & editing, Writing – original draft, Visualization, Validation, Project administration, Methodology, Investigation, Funding acquisition, Formal analysis, Data curation, Conceptualization. **Annabelle T. Fricker:** Resources, Methodology, Investigation. **Rafał Konefał:** Resources, Methodology, Investigation, Formal analysis. **Aneta Medaj:** Visualization, Investigation, Formal analysis. **Małgorzata Zimowska:** Visualization, Investigation. **Bartosz Leszczyński:** Visualization, Investigation. **Andrzej Wróbel:** Visualization, Investigation. **Andrzej J. Bojarski:** Writing – review & editing, Supervision. **Ipsita Roy:** Writing – review & editing, Supervision, Resources, Methodology. **Maciej Guzik:** Writing – review & editing, Supervision, Resources, Project administration, Funding acquisition, Conceptualization.

Declaration of competing interest

The authors declare that they have no known competing financial interests or personal relationships that could have appeared to influence the work reported in this paper.

Data availability

The data presented in this study are available on request from the corresponding author.

Acknowledgements

Research funded by The National Centre for Research and Development, grant Lider. no. LIDER/27/0090/L-7/15/NCBR/2016. K.H. acknowledges the financial support from the National Agency for Academic Exchange under the Iwanowska programme (scholarship no. PPN/IWA/2019/1/00228/U/00001), and under the PROM programme no. PPI/PRO/2019/1/00021/4/PROM/2022. K.H. was partially supported by the InterDokMed project, no. POWR.03.02.00-00-I013/16. We would like to thank greatly Karolina Stępień for performing tests related to the determination of the antimicrobial activity for synthesised compounds.

Appendix A. Supplementary data

The Supporting Information presents: (1) list of materials used; (2) methodologies for (a) selection of the most favourable reaction parameters for preparation of Dic-oligo(3HAs), and (b) synthesis of blends containing Dic-oligo(3HAs); (3) Methods: (a) Spectroscopic analysis of Dic-oligo(3HAs): ^{13}C NMR, ^{1}H–^{1}H (correlation spectroscopy – COSY), ^{1}H–^{13}C (single heteronuclear quantum coherence spectroscopy – HSQC), ^{1}H–^{13}C (multiple heteronuclear quantum coherence spectroscopy – HMBC), and mass spectrometric (MS) analyses; (b) Dic releasing experiments; (c) the release kinetics; (d) determination of the wettability and surface free energy; (e) structural analysis of prepared foams: computed microtomography (μ-CT), atomic force microscopy (AFM), and mechanical tests; (f) biological tests in vitro: cell culture conditions for human keratinocytes (HaCaT), resazurin spectrophotometric assay, and direct bioassays performed in contact with the surface of biomaterials; (4) Results of: (a) ^{1}H NMR analyses, (b) ^{13}C NMR analysis of final mixture [Dic-oligo(3HAs)]; (c) COSY, (d) HMBC, (e) HSQC, (f) MS, (g) graphs and results regarding to release experiments, (h) parameters for the kinetic models used, (i) the wettability of P(3HO) and P(3HO)/Dic-oligo(3HAs), (j) the surface energy of P(3HO) and P(3HO)/Dic-oligo(3HAs), (k) the reconstructed cross-sections of prepared patches, (l) the distribution of pore diameters in the prepared patches, (m) Young's modulus, tensile strength and elongation at break of prepared patches, (n) the proliferation rate of HaCaT cells on the surface of the tested biomaterials. Supplementary data to this article can be found online at https://doi.org/10.1016/j.ijbiomac.2024.131476.

References

[1] G. Kaur, G. Narayanan, D. Garg, A. Sachdev, I. Matai, Biomaterials-based regenerative strategies for skin tissue wound healing, ACS Applied Biomaterials 5 (2022) 2069–2106, https://doi.org/10.1021/acsabm.2c 00035.

[2] X. Deng, M. Gould, M.A. Ali, A review of current advancements for wound healing : biomaterial applications and medical devices, J. Biomed. Mater. Res. 110 (2022) 2542–2573, https://doi.org/10.1002/jbm.b. 35086.

[3] A.L. Alessandri, L.P. Sousa, C.D. Lucas, A.G. Rossi, V. Pinho, M.M. Teixeira, Resolution of inflammation : mechanisms and opportunity for drug development, Pharmacol. Ther. 139 (2) (2013) 189–212, https://doi.org/10.1016/j.pharmthera.2013.04.006.

[4] J.M. Al-Khayri, G.R. Sahana, P. Nagella, B.V. Joseph, F.M. Alessa, M.Q. Al-Mssallem, Flavonoids as potential anti-inflammatory molecules : a review, Molecules 27 (2901) (2022) 1–24.

[5] L. Pereira, S. Oliveira, J. Almeida, J. Maísa, B.P. Rocha, P.De. Lucena, A review on developments and prospects of anti-inflammatory in microemulsions, J Drug Deliv Sci Technol 60 (102008) (2020) 1–14, https://doi.org/10.1016/j.jddst.2020.102008.

[6] F.L. de S. Costa, L.D. Tiussi, M.S. Nascimento, A.C. de S. Correa, E.Y. Yasojima, C.A. A. Pires, Diclofenac topical gel in excisional wounds maintain heal quality and reduce phlogistic signals 1, Acta Chirurgica Brasileira vol. 29 (5) (2014) 328–333.

[7] K.S. Postolovic, M.D. Antonijevic, B. Ljujic, S. Radenkovic, M.M. Kovacevic, Z. Hiezl, S. Pavlovic, I. Radojevic, Z. Stanic, Curcumin and diclofenac therapeutic efficacy enhancement applying transdermal hydrogel polymer films, Based On. Polymers (Basel) 14 (4091) (2022) 1–27.

[8] K. Vig, A. Chaudhari, S. Tripathi, S. Dixit, R. Sahu, S. Pillai, V.A. Dennis, S.R. Singh, Advances in skin regeneration using tissue engineering, Int. J. Mol. Sci. 18 (2017) 789, https://doi.org/10.3390/ijms18040789.

[9] A. Przekora, A concise review on tissue engineered artificial skin grafts for chronic wound treatment : can we reconstruct functional skin tissue in vitro ? Cells 9 (4) (2020) 1–29, https://doi.org/10.3390/cells9071622.

[10] T. Garg, O. Singh, S. Arora, R.S.R. Murthy, Scaffold : a novel carrier for cell and drug delivery, Crit. Rev. Ther. Drug Carrier Syst. 29 (1) (2012) 1–63, https://doi.org/10.1615/CritRevTherDrugCarrierSyst.v29.i1.10.

[11] C. Utsunomia, Q. Ren, M. Zinn, Poly(4-Hydroxybutyrate): current state and perspectives, Front. Bioeng. Biotechnol. 8 (257) (2020) 1–18, https://doi.org/10.3389/fbioe.2020.00257.

[12] E. Cichoń, K. Haraźna, S. Skibiński, T. Witko, A. Zima, A. Ślósarczyk, M. Zimowska, M. Witko, B. Leszczyński, A. Wróbel, M. Guzik, Novel bioresorbable tricalcium phosphate/polyhydroxyoctanoate (TCP/PHO) composites as scaffolds for bone tissue engineering applications, J. Mech. Behav. Biomed. Mater. 98 (2019) 235–245, https://doi.org/10.1016/j.jmbbm.2019.06.028.

[13] D.A. Gregory, A.T.R. Fricker, P. Mitrev, M. Ray, E. Asare, D. Sim, S. Larpnimitchai, Z. Zhang, J. Ma, S.S.V. Tetali, I. Roy, Additive manufacturing of polyhydroxyalkanoate-based blends using fused deposition modelling for the development of biomedical devices, J Funct Biomater 14 (1) (2023), https://doi.org/10.3390/jfb14010040.

[14] C.S. Taylor, M. Behbehani, A. Glen, P. Basnett, D.A. Gregory, B.B. Lukasiewicz, R. Nigmatullin, F. Claeyssens, I. Roy, J.W. Haycock, Aligned polyhydroxyalkanoate blend electrospun fibers as intraluminal guidance scaffolds for peripheral nerve repair, ACS Biomater Sci. Eng. 9 (3) (2023) 1472–1485, https://doi.org/10.1021/acsbiomaterials.2c00964.

[15] D. Ahmed, H. Puthussery, P. Basnett, J.C. Knowles, S. Lange, I. Roy, Controlled delivery of Pan-PAD-inhibitor Cl-amidine using poly(3-hydroxybutyrate) microspheres, Int. J. Mol. Sci. 22 (23) (2021), https://doi.org/10.3390/ijms222312852.

[16] R. Nigmatullin, C.S. Taylor, P. Basnett, B. Lukasiewicz, A. Paxinou, L.R. Lizarraga-Valderrama, J.W. Haycock, I. Roy, Medium chain length polyhydroxyalkanoates as potential matrix materials for peripheral nerve regeneration, Regen Biomater (2023) 10, https://doi.org/10.1093/rb/rbad063.

[17] P. Basnett, R.K. Matharu, C.S. Taylor, U. Illangakoon, J.I. Dawson, J.M. Kanczler, M. Behbehani, E. Humphrey, Q. Majid, B. Lukasiewicz, R. Nigmatullin, P. Heseltine, R.O.C. Oreffo, J.W. Haycock, C. Terracciano, S.E. Harding, M. Edirisinghe, I. Roy, Harnessing polyhydroxyalkanoates and pressurized gyration for hard and soft tissue engineering, ACS Appl. Mater. Interfaces 13 (28) (2021) 32624–32639, https://doi.org/10.1021/acsami.0c19689.

[18] B. Azimi, L. Thomas, A. Fusco, O.I. Kalaoglu-Altan, P. Basnett, P. Cinelli, K. de Clerck, I. Roy, G. Donnarumma, M.B. Coltelli, S. Danti, A. Lazzeri, Electrosprayed chitin nanofibril/electrospun polyhydroxyalkanoate fiber mesh as functional nonwoven for skin application, J Funct Biomater (2020) 11 (3), https://doi.org/10.3390/jfb11030062.

[19] A. Tomar, P. Uysal-Onganer, P. Basnett, U. Pati, I. Roy, 3D disease modelling of hard and soft cancer using PHA-based scaffolds, Cancers (Basel) 14 (14) (2022), https://doi.org/10.3390/cancers14143549.

[20] O.I. Kalaoglu-Altan, H. Baskan, T. Meireman, P. Basnett, B. Azimi, A. Fusco, N. Funel, G. Donnarumma, A. Lazzeri, I. Roy, S. Danti, K. De Clerck, Silver nanoparticle-coated polyhydroxy- alkanoate based electrospun fibers for wound dressing applications, Materials 14 (17) (2021), https://doi.org/10.3390/ma14174907.

[21] S. Skibiński, E. Cichoń, K. Haraźna, E. Marcello, I. Roy, M. Witko, A. Ślósarczyk, J. Czechowska, M. Guzik, A. Zima, Functionalized tricalcium phosphate and poly (3-hydroxyoctanoate) derived composite scaffolds as platforms for the controlled release of diclofenac, Ceram. Int. (2020), https://doi.org/10.1016/j.ceramint.2020.09.248.

[22] A.C. Ward, P. Dubey, P. Basnett, G. Lika, G. Newman, D.K. Corrigan, C. Russell, J. Kim, S. Chakrabarty, P. Connolly, I. Roy, Toward a closed loop, integrated biocompatible biopolymer wound dressing patch for detection and prevention of chronic wound infections, Front. Bioeng. Biotechnol. 8 (1039) (2020) 1–12, https://doi.org/10.3389/fbioe.2020.01039.

[23] X.-T. Li, Y. Zhang, G.-Q. Chen, Biomaterials nanofibrous polyhydroxyalkanoate matrices as cell growth supporting materials, Biomaterials 29 (2008) 3720–3728, https://doi.org/10.1016/j.biomaterials. 2008.06.004.

[24] K. Sofińska, J. Barbasz, T. Witko, J. Dryzek, K. Haraźna, M. Witko, J. Kryściak-Czerwenka, M. Guzik, Structural, topographical, and mechanical characteristics of purified polyhydroxyoctanoate polymer, J. Appl. Polym. Sci. 136 (4) (2019) 47192, https://doi.org/10.1002/app.47192.

[25] K. Haraźna, E. Cichoń, S. Skibiński, T. Witko, D. Solarz, I. Kwiecień, E. Marcello, M. Zimowska, R. Socha, E. Szefer, A. Zima, I. Roy, K.N. Raftopoulos, K. Pielichowski, M. Witko, M. Guzik, Physicochemical and biological characterisation of diclofenac oligomeric poly(3-hydroxyoctanoate) hybrids as β-TCP ceramics modifiers for bone tissue regeneration, Int. J. Mol. Sci. (2020) 1–23, https://doi.org/10.3390/ijms21249452.

[26] M. Seta, K. Haraźna, K. Kasarełło, D. Solarz-Keller, A. Cudnoch-Jędrzejewska, T. Witko, Z. Rajfur, M. Guzik, The influence of novel, biocompatible, and bioresorbable poly (3-hydroxyoctanoate) dressings on wound healing in mice, Int. J. Mol. Sci. 23 (16159) (2022) 1–29.

[27] D.A. Gregory, C.S. Taylor, A.T.R. Fricker, E. Asare, S.S.V. Tetali, J.W. Haycock, I. Roy, Polyhydroxyalkanoates and their advances for biomedical applications, Trends Mol. Med. 28 (4) (2022) 331–342, https://doi.org/10.1016/j.molmed.2022.01.007.

[28] C. Durairaj, S.J. Kim, H.F. Edelhauser, J.C. Shah, B. Kompella, Influence of dosage form on the intravitreal pharmacokinetics of diclofenac, Invest. Ophthalmol. Vis. Sci. 50 (10) (2009) 4887–4897, https://doi.org/10.1167/iovs.09-3565.Influence.

[29] A. Chiarini, A. Tartarini, A. Fini, PH-solubility relationship and partition coefficients for some anti-inflammatory arylaliphatic acids, Arch Pharm (Weinheim) 273 (1984) 268–273.

[30] D. Wójcik-Pastuszka, J. Krzak, B. Macikowski, R. Berkowski, B. Osiński, W. Musiał, Evaluation of the release kinetics of a pharmacologically active substance from model intra-articular implants replacing the cruciate ligaments of the knee, Materials 12 (1202) (2019) 1–13.

[31] V. Dash, S.K. Mishra, M. Singh, A.K. Goyal, G. Rath, Release kinetic studies of aspirin microcapsules from ethyl cellulose, cellulose acetate phthalate and their mixtures by emulsion solvent evaporation method, Sci. Pharm. 78 (2010) 93–101, https://doi.org/10.3797/scipharm.0908-09.

[32] C. Jantarat, P. Muenraya, S. Srivaro, A. Nawakitrangsan, K. Promsornpason, Comparison of drug release behavior of bacterial cellulose loaded with ibuprofen and propranolol hydrochloride, RSC Adv. 11 (2021) 37354–37365, https://doi.org/10.1039/d1ra07761a.

[33] S. Kini, D. Bahadur, D. Panda, Mechanism of anti-cancer activity of benomyl loaded nanoparticles in multidrug resistant cancer cells, J. Biomed. Nanotechnol. 2014 (10) (1998) 1–13, https://doi.org/10.1166/jbn.2015.

[34] B. Iqbal, M. Pharm, J. Ali, M. Pharm, S. Baboota, M. Pharm, Recent advances and development in epidermal and dermal drug deposition enhancement technology, Int. J. Dermatol. 57 (6) (2018) 646–660, https://doi.org/10.1111/ijd.13902.

[35] M. Brunner, P. Dehghanyar, B. Seigfried, W. Martin, G. Menke, M. Müller, Favourable dermal penetration of diclofenac after administration to the skin using a novel spray gel formulation, Br. J. Clin. Pharmacol. 60 (5) (2005) 573–577, https://doi.org/10.1111/j.1365-2125.2005.02484.x.

[36] D. Paolino, A. Tudose, C. Celia, L. Di Marzio, F. Cilurzo, C. Mircioiu, Mathematical models as tools to predict the release kinetic of fluorescein from Lyotropic colloidal liquid crystals, Materials 12 (693) (2019) 1–23, https://doi.org/10.3390/ma12050693.

[37] C.P. Jara, N. Mendes, T.P. Do Prado, E.P. Araujo, Bioactive fatty acids in the resolution of chronic inflammation in skin wounds, Advanced in Wound Care (2019) 1–47, https://doi.org/10.1089/wound.2019.1105.

[38] A. Sioufi, F. Pommier, F. Boschet, J. Godbillon, D. Lavoignat, D. Salliere, Percutaneous absorption of diclofenac in healthy volunteers after single and repeated topical application of diclofenac emulgel, Biopharm. Drug Dispos. 15 (1994) 441–449.

[39] E.H. Ukomadu, M. Sacha, A. Richter, K. Hussein, Hydrogel increases diclofenac skin permeation and absorption, Biopharmaceutics and drug deposition 40 (2019) 217–224, https://doi.org/10.1002/bdd.2194.

[40] C. Mohanty, M. Das, S.K. Sahoo, Sustained wound healing activity of curcumin loaded oleic acid based polymeric bandage in a rat model, Mol. Pharm. 9 (2012) 2801–2811.

[41] T. Maver, S. Hribernik, T. Mohan, M. Smrke, Functional wound dressing materials with highly tunable drug release properties, RSC Adv. 5 (2015) 77873–77884, https://doi.org/10.1039/c5ra11972c.

[42] Z.A. Mirani, S. Naz, F. Khan, M. Aziz, M.N. Khan, Antibacterial fatty acids destabilize hydrophobic and multicellular aggregates of bio fi lm in *S. aureus*, J Antibiot (Tokyo) 70 (2017) 115–121, https://doi.org/10.1038/ja.2016.76.

[43] R. Serra, R. Grande, L. Butrico, A. Rossi, B. Caroleo, B. Amato, L. Gallelli, S. De. Franciscis, Chronic wound infections : the role of pseudomonas aeruginosa and Staphylococcus aureus, Expert Rev. Dermat. 13 (5) (2015) 605–613.

[44] R.C. Paes Leme, R.B. da Silva, Antimicrobial activity of non-steroidal anti-inflammatory drugs on biofilm: current evidence and potential for drug repurposing, Front. Microbiol. 12 (2021), https://doi.org/10.3389/fmicb.2021.707629.

[45] C.M. Ferrer-Luque, C. Solana, B. Aguado, M. Ruiz-Linares, Antimicrobial activity and cytotoxicity of nonsteroidal anti-inflammatory drugs against endodontic biofilms, Antibiotics 12 (3) (2023), https://doi.org/10.3390/antibiotics12030450.
[46] A. Ullah, M.N. Sarwar, F. fei Wang, D. Kharaghani, L. Sun, C. Zhu, Y. Yoshiko, G. Mayakrishnan, J.S. Lee, I.S. Kim, In vitro biocompatibility, antibacterial activity, and release behavior of halloysite nanotubes loaded with diclofenac sodium salt incorporated in electrospun soy protein isolate/ hydroxyethyl cellulose nanofibers, Curr Res Biotechnol vol. 4 (2022) 445–458, https://doi.org/10.1016/j.crbiot.2022.09.008.
[47] J. Liu, Medical Adhesives and Skin Adhesion, 1993.
[48] V. Sharma, N. Patel, N. Kohli, N. Ravindran, L. Hook, C. Mason, Viscoelastic, physical, and bio-degradable properties of dermal scaffolds and related cell behaviour, Biomed. Mater. 11 (055001) (2016) 1–12, https://doi.org/10.1088/1748-6041/11/5/055001.
[49] A.A. Chaudhari, K. Vig, D.R. Baganizi, R. Sahu, S. Dixit, V. Dennis, S.R. Singh, S. R. Pillai, Future prospects for scaffolding methods and biomaterials in skin tissue engineering: a review, Int. J. Mol. Sci. 2016 (17) (1974) 1–31, https://doi.org/10.3390/ijms17121974.
[50] L. Huang, J. Huang, H. Shao, X. Hu, C. Cao, S. Fan, L. Song, Silk scaffolds with gradient pore structure and improved cell infiltration performance, Mater. Sci. Eng. C 94 (2019) 179–189, https://doi.org/10.1016/j.msec.2018.09.034.
[51] A. Kalra, A. Low, A.Al. Jumaily, An overview of factors affecting the skin's Young's modulus, Journal of Ageing Science 4 (2) (2016) 1–5, https://doi.org/10.4172/2329-8847.1000156.
[52] A. Annaidh, K. Bruyère, M. Destrade, M.D. Gilchrist, Characterization of the anisotropic mechanical properties of excised human skin, J. Mech. Behav. Biomed. Mater. 5 (1) (2012) 139–148, https://doi.org/10.1016/j.jmbbm.2011.08.016.
[53] M. Rahmati, J.J. Blaker, S.P. Lyngstadaas, J.F. Mano, H.J. Haugen, Designing multigradient biomaterials for skin regeneration, Mater Today Adv 5 (2020) 100051, https://doi.org/10.1016/j.mtadv.2019.100051.
[54] M. Wojcik, P. Kazimierczak, V. Vivcharenko, M. Koziol, A. Przekora, Effect of vitamin C/hydrocortisone immobilization within curdlan-based wound dressings on in vitro cellular response in context of the management of chronic and burn wounds, Int. J. Mol. Sci. 22 (11474) (2021) 1–16.